Bulletin of the Seismological Society of America, Vol. 97, No. 1A, pp. S271–S278, January 2007, doi: 10.1785/0120050625

Loading and Gravitational Effects of the 2004 Indian Ocean Tsunami at Syowa Station, Antarctica

by Kazunari Nawa, Naoki Suda, Kenji Satake, Yushiro Fujii, Tadahiro Sato, Koichiro Doi, Masaki Kanao, and Kazuo Shibuya

Abstract The 2004 Indian Ocean tsunami reached Syowa Station, Antarctica, approximately 12.5 hr after the December Sumatra–Andaman earthquake. We have analyzed the tsunami signals recorded on ocean-bottom pressure gauges, broadband seismometers (STS-1), and a superconducting gravimeter (SG). We calculated the sea level variation, tilt, and gravity changes induced by the tsunami and compared these results to observations. From this comparison we confirmed the loading and gravity effects of the tsunamis on the STS-1 (horizontal components) and the SG records at Syowa Station. The magnitudes of these effects given as root mean square amplitudes are as follows: for the tilt effects obtained from 20-hr-long STS-1 records at frequencies in the range 0.3–0.6 mHz, 5 and 8 μGal (10^{-8} m/sec^2) in the east–west and north–south directions, respectively; and for the gravity effect obtained from the SG records for the same time period of 20 hr at frequencies in the range 0.1–0.2 mHz, 0.2 μGal. By using detailed bathymetry around Syowa Station, the synthetic amplitudes similar to the observed were obtained, although the waveforms of synthetic and observation are not always consistent.

Introduction

The 2004 Indian Ocean tsunami generated by the Sumatra–Andaman earthquake reached the global oceans (Merrifield *et al.*, 2005; Titov *et al.*, 2005) and also affected the atmosphere and the solid Earth at the ocean surface and floor, respectively. Coupled phenomena of the tsunami were detected by various sensors, such as microbarometers and magnetometers of the atmosphere (e.g., Iyemori *et al.*, 2005; Le Pichon *et al.*, 2005), and seismometers of the solid Earth (Hanson and Bowman, 2005; Yuan *et al.*, 2005).

Yuan *et al.* (2005) describe detection of the tsunami effect on broadband seismometers installed at islands and coastal regions of the Indian Ocean and reported that the possible cause was land tilt due to ocean loading. Prior to the 2004 tsunamis there were few reports of tsunami effects detected at seismic, or geodetic, stations. For instance, tsunami effects were detected at observation sites close to the source region of the 2002 Stromboli Volcano landslides (Pino *et al.*, 2004) and of the 1983 Nihonkai–Chubu Earthquake (Yanagisawa and Wakasugi, 1984). On the geodetic records, at distances over several thousands kilometers from the source, the tsunami loading effects of the 1960 Chilean earthquake were detected in Japan (Ozawa, 1961; Tanaka and Tanaka, 1961). However, after the Chilean earthquake there have been no similar reports of tsunami loading observations at seismic, or geodetic, stations at large distances from the source.

Two ocean-bottom pressure gauges, one (BPG1) at Syowa Station, Antarctica (69° S 39.6° E) (Odamaki *et al.*, 1991), and the other (BPG2) on the ocean floor in the Antarctic Ocean (66.9° S, 37.8° E) near the station (Doi *et al.*, 2005) recorded the Indian Ocean tsunami approximately 12.5 hr after the earthquake. This is the first observation of a tsunami on sea level gauges by the Japanese Antarctic Research Expedition (JARE) since 1976 (Odamaki *et al.*, 2005). The broadband seismometers (STS-1) and a superconducting gravimeter (SG) at Syowa Station also recorded the loading and gravitational effects of the tsunami as well as the seismic waves of the 2004 Sumatra–Andaman earthquake.

It is important to study the tsunami effects observed at seismic and/or geodetic stations for the (1) availability of new data types, in addition to sea level data, for the study of the tsunami and seismic source mechanism, (2) estimation of the subsurface structure in response to ocean loading, and (3) noise reduction in the analysis of seismic waves, in particular low-frequency modes of the Earth's free oscillations, as demonstrated by Nawa *et al.* (2003). In this article, a first step of such studies as aforementioned, we compute the synthetic waves based on realistic models (with source and bathymetry) and compare them to the observations of STS-1 and SG at Syowa Station.

Observation

Syowa Station is on East Ongul Island at the mouth of Lützow–Holm Bay in the coastal region of Antarctica (Fig. 1). Continuous sea level observations are ongoing at the Nisi-no-ura Cove by the Japan Coast Guard with an ocean-bottom pressure gauge (at BPG1 shown in Fig. 1b). A new ocean-bottom pressure gauge (BPG2) was installed on 15 December 2004 by the forty-sixth JARE in the Antarctic Ocean (Fig. 1a), which has recorded data for more than 50 days, including the 2004 Indian Ocean tsunami (Doi *et al.*, 2005).

The STS-1 observations have continued since 1990, and the SG observations since 1993. In 1997, STS-1 seismometers were reinstalled at a new seismological observation hut (Kanao *et al.*, 1999). A new type of SG, compact in size and employing a bottom mount (CT#043), replaced the old regular size, top mounted SG (TT70#016) in 2003 (Fukuda *et al.*, 2005; Ikeda *et al.*, 2005). The distance between the STS-1 and SG sites is less than 50 m. And the distances between these two sites and the nearest coast are less than 200 m (Fig. 1b). The sampling intervals of the BPG1, STS-1, and SG are 30 sec, 0.05 sec, and 1 sec, respectively.

The instruments recorded the signals from the 2004 Sumatra–Andaman earthquake (Fig. 2). In Figure 2b the bandpass-filtered waveforms in the frequency range 0.3–1.5 mHz with the tidal components removed are presented. The tsunami arrived at Syowa Station 12 hr and 40 min after the 2004 Sumatra–Andaman earthquake. In records of the STS-1 north–south and east–west components, tsunami-like waveforms are clearly observed after arrival on BPG1. In records of vertical components, that is STS-1 Z and SG, it is difficult to resolve the tsunami effects in the time domain. However, as shown later, the tsunami effects are observed in a limited frequency band.

Sea Level Variation by the 2004 Indian Ocean Tsunami

Modeling

In order to calculate the tilt and gravity effects of the tsunami, we first need to calculate the tsunami waveforms of the global ocean. Initial water height distribution is computed using the tsunami source model inferred from tide gauge and satellite data by Fujii and Satake (2007). Tsunami waveforms are computed by assuming linear long waves and using the finite-difference method. The details of the tsunami computation method are described in Satake (2002). The grid size of the computation is 10 min of the arc. The bathymetry grid was made from a global digital topography data set compiled from ETOPO2 (National Oceanic and Atmospheric Administration [NOAA], 2001).

Figure 3 illustrates the water height distribution of a simulated Indian Ocean tsunami at 12.5 hr after the 2004 Sumatra–Andaman earthquake. Using this water-height distribution data, we computed the tsunami loading and gravitational effects in the horizontal and vertical directions at Syowa Station.

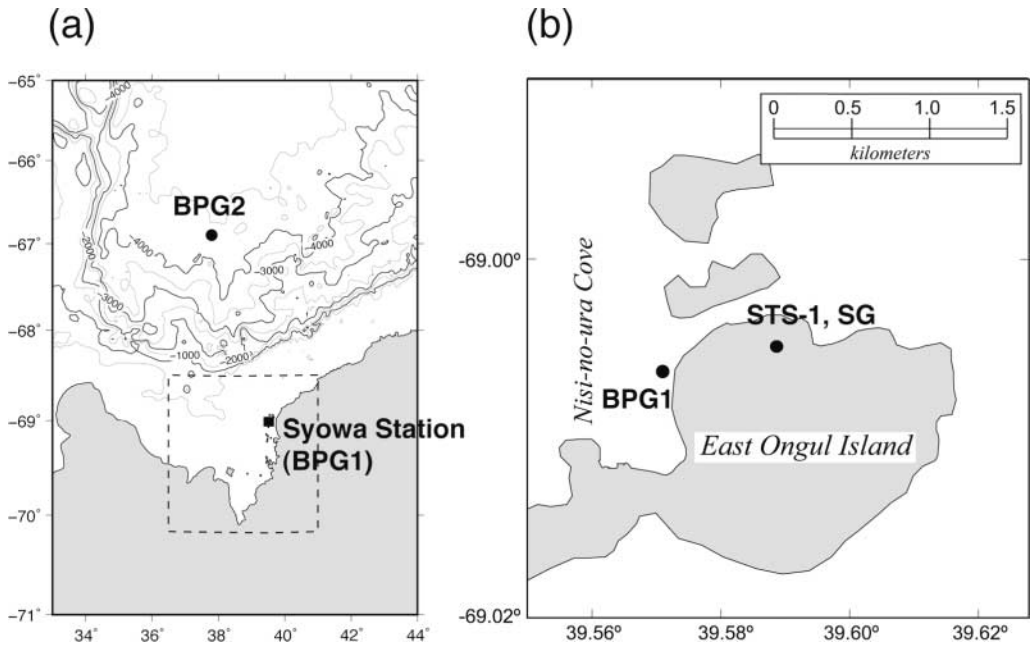

Figure 1. Location of the observation sites. (a) Maps of the vicinity of Lützow–Holm Bay; (b) Syowa Station on East Ongul Island. BPG1 (BPG2), STS-1, and SG denote the locations of the ocean-bottom pressure gauges, broadband seismometer, and the superconducting gravimeter, respectively. A rectangle in (a) highlights the area of the detailed bathymetry model used to calculate the synthetic waveforms (see Fig. 6).

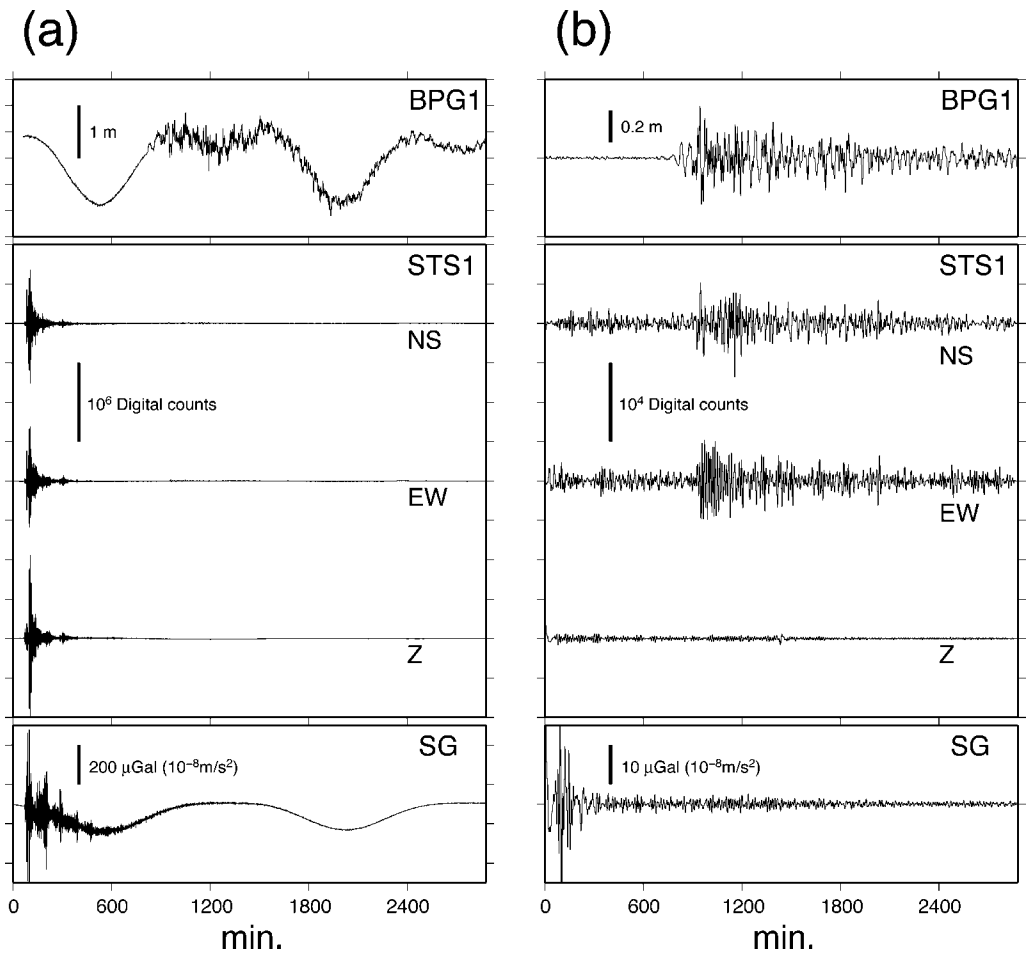

Figure 2. (a) Raw data and (b) filtered data in the frequency range 0.3–1.5 mHz of sea level (BPG1), ground velocity (STS1), and gravity (SG). Time is measured from the origin time of the 2004 Sumatra–Andaman earthquake.

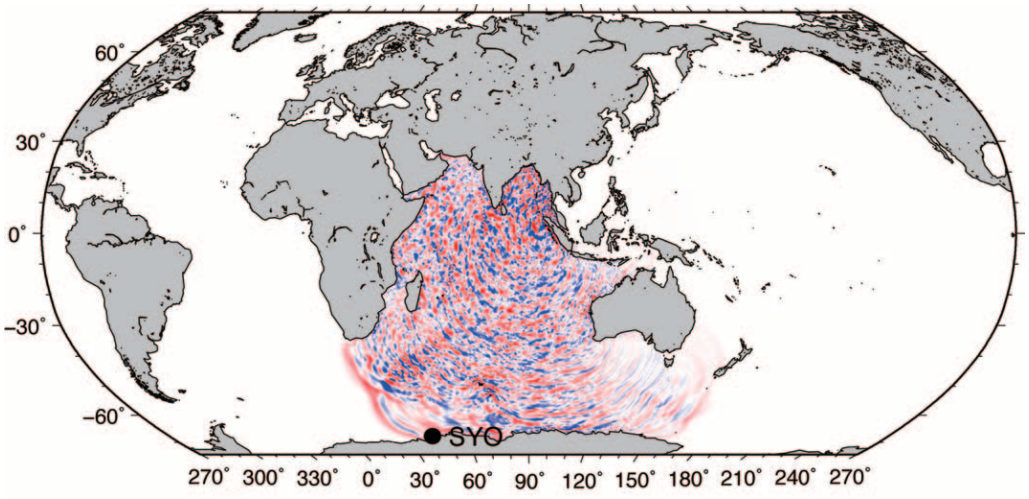

Figure 3. Water height distribution of the simulated Indian Ocean tsunami 12.5 hr after the 2004 Sumatra–Andaman earthquake. Red color denotes a water height higher than normal, while blue denotes lower. Initial water height distribution is calculated employing the source model inferred by Fujii and Satake (2007). SYO denotes the location of Syowa Station (69° S, 39.6° E).

Comparison with Sea Level Data

Before calculating the tsunami effects on the solid Earth, we compare the synthetic tsunami calculated using ETOPO2 bathymetry, with the observed records at BPG1 and BPG2. Figure 4 shows the power spectral densities (PSDs) and filtered time series for a limited frequency band of the synthetic tsunamis and observations. Sampled data at 1 min are presented for both records of BPG1 and BPG2.

At both sites, the PSDs of the synthetic and observation are found to be comparable in magnitude at lower frequencies, although the spectral shapes are not quite the same. At BPG2, located at the deep ocean floor (>4000 m), PSDs of the synthetic are comparable to those of observation up to a frequency of approximately 3 mHz. However, from BPG1 at a shallower depth, the PSDs of synthetic and observation differ at frequencies higher than 1 mHz; this is probably due to the inaccuracy of the modeled bathymetry data and smaller grid size of computation for reproducing the tsunami at Syowa Station. The accuracy of bathymetry data will be discussed in the following sections.

Since the discrepancy of PSDs between the synthetic and observation is large at frequencies higher than 1 mHz, we applied a bandpass filter (0.3–0.6 mHz) to the observed data at Syowa Station and compared this data with the synthetics in the same frequency band (Fig. 4). Onsets of the synthetic tsunamis agree with those of the observations. Mean amplitudes of the synthetic tsunamis are comparable to those of the observed tsunamis. In the comparison of the synthetics and observed data for sea level and tilt variations in the following section we apply a bandpass filter at the same frequency to all data.

Tilt and Gravity Variations at Syowa Station

Calculation of Synthetic Waveforms

We computed the tilt and gravity variation at Syowa Station induced by the tsunami and compared the results with observations. The attraction and loading (elastic) effects in the horizontal and vertical directions were calculated using a modified version of GOTIC (a program for Global Oceanic Tidal Correction by Sato and Hanada [1984]) every 5 min for two days after the earthquake.

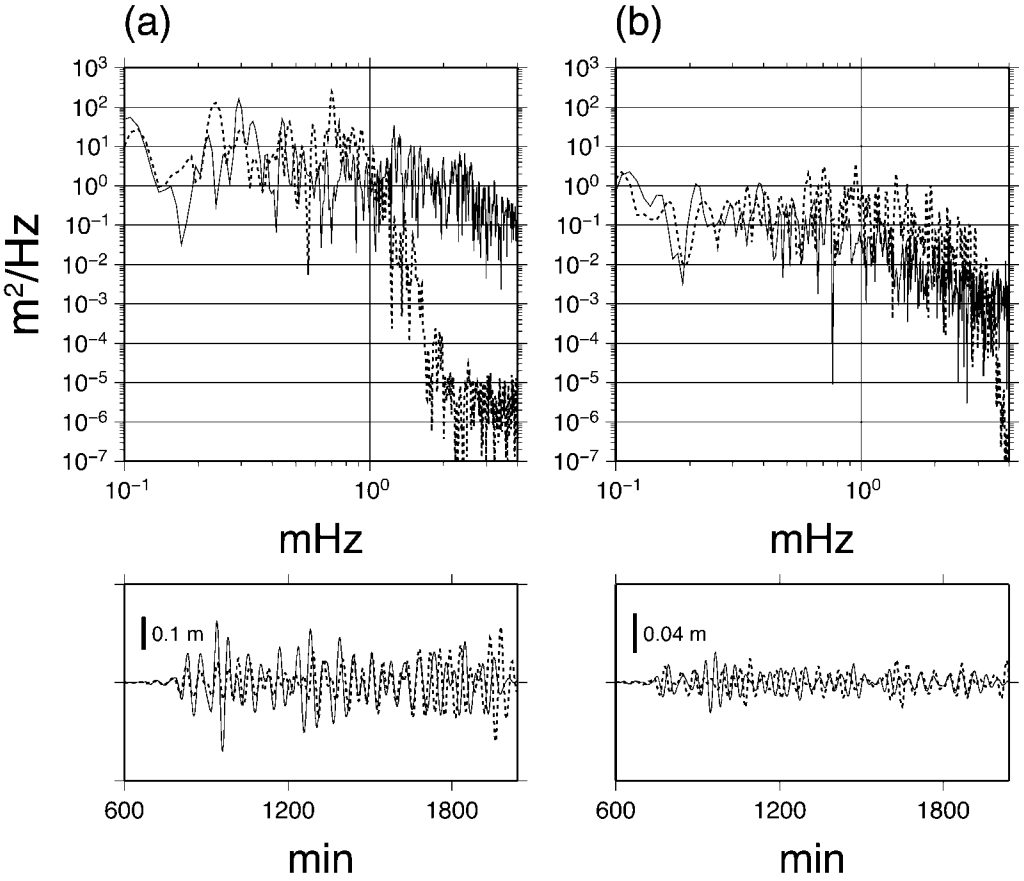

Figure 4. A comparison of observed (solid curves) and synthetic (dashed curves) tsunami data at (a) BPG1 and (b) BPG2. Top panels are the comparison of spectra and bottom panels are the comparison of the time series, filtered in the frequency range 0.3–0.6 mHz. Time is measured from the origin time of the 2004 Sumatra–Andaman earthquake.

The GOTIC is based on Farrell's convolution method (Farrell, 1972). The computation was performed by integrating a convolution of the mass change due to the synthetic global water height variations (Fig. 3) and a Green's function of the loading for the 1066A Earth model over the Indian Ocean (Endo and Okubo, 1984).

We summarize the comparison between synthetics and observations in Figure 5 and Table 1. Synthetic waves were calculated in two cases using bathymetry: one based only on ETOPO2 data (Fig. 5a) and the other merged with water depth data digitized from a bathymetric chart of Lützow–Holm Bay (Moriwaki and Yoshida, 1990) (Fig. 5b).

Tilt Components and STS-1H Records

We compared the STS-1H records with the synthetic tilt in the frequency range 0.3–0.6 mHz. For the comparison the STS-1H records were converted to acceleration from the original velocity data corrected for sensor response. The unit of synthetic tilt variation (t) was converted to acceleration (a), using the relation

$$a = -9.8 \sin(t),$$

where 9.8 is the assumed acceleration value due to gravity (m/sec^2).

As presented in Figure 5, STS-1H detected the tsunami effects as a tilt, including the change in the gravitational attraction caused by the ocean mass changes. The observed amplitude of STS-1H is comparable to that of the synthetic waveform. In Figure 5a, the case using only ETOPO2 for the bathymetry, the root mean square amplitudes of the north–south component in the period from 760 to 1960 min are 7.9 μGal (10^{-8} m/sec^2) for the observation and 20.1 μGal for the synthetic. The amplitudes of the east–west component are 4.7 μGal for the observation and 10.6 μGal for the synthetic.

An observed characteristic of the larger north–south component (compared to the east–west component) is also synthesized. The observations show that the north–south component, perpendicular to the coastline (Fig. 1b), is dominant, as reported from other sites in and around the Indian Ocean (Yuan *et al.*, 2005). Quantitatively, synthetic amplitudes of both components are slightly larger than the observed amplitudes. As we will discuss subsequently, this situation depends on the bathymetric data used for the calculation.

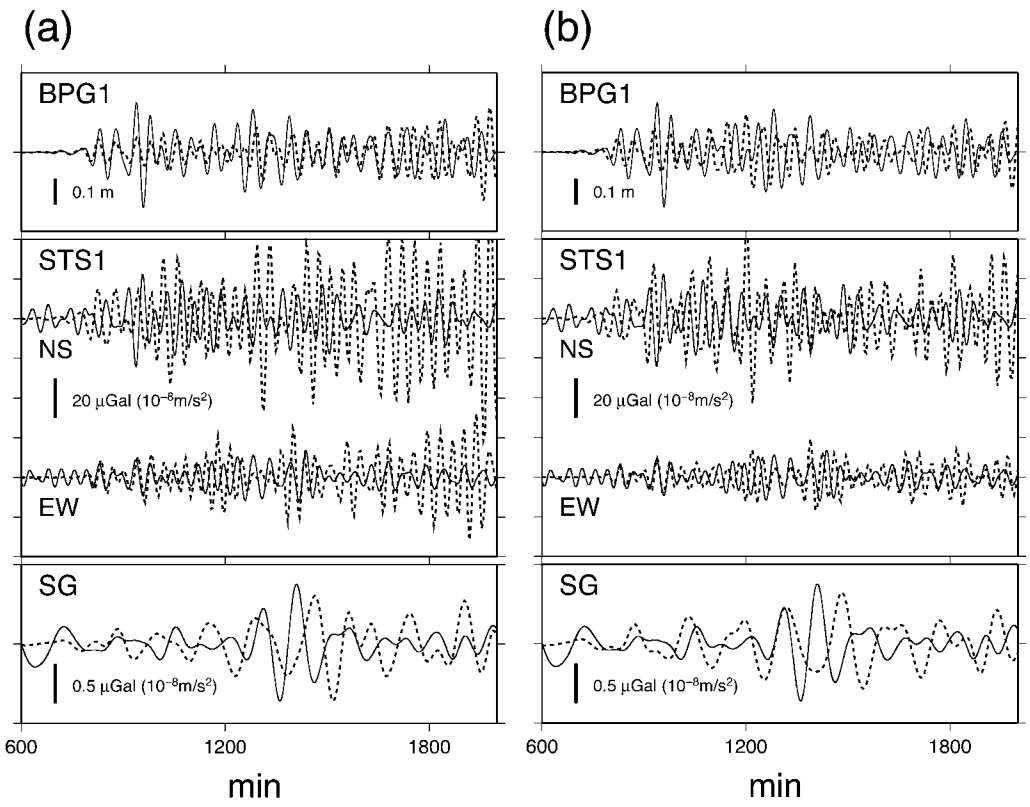

Figure 5. A comparison of observed (solid curves) and synthetic (dashed curves) waveforms. Time is measured from the origin time of the 2004 Sumatra–Andaman earthquake. Synthetic waveforms are calculated using different bathymetric models: (a) ETOPO2 and (b) ETOPO2 and detailed bathymetry. The waveform of BPG1 and STS1 are filtered in the frequency range 0.3–0.6 mHz. However, the waveform of SG is in the frequency range 0.1–0.2 mHz. See text for the details.

Table 1
Amplitudes of Observed and Synthetic Waveforms from 760 to 1960 Min

	Observed	Synthetic a	Synthetic b
BPG1 (m)	0.066	0.050	0.049
STS-1 NS (μGal)	7.9	20.1	14.4
STS-1 EW (μGal)	4.7	10.6	6.2
SG (μGal)	0.20	0.25	0.26

Synthetic a is computed from ETOPO2 bathymetry and synthetic b is for ETOPO2 plus more detailed bathymetry around Syowa Station. Waveforms of BPG1 and STS-1 were bandpass filtered at frequencies in the range 0.3–0.6 mHz and that of SG data was filtered at frequencies in the range 0.1–0.2 mHz.

Gravity Components and SG Records

Tsunami effects are smaller in the vertical component, compared to the horizontal component, in acceleration. In addition, the frequencies of the tsunami effects overlap those of the Earth's free oscillations. The magnitude of the tsunami effects is comparable to those of the free oscillations. In order to extract the tsunami effects and remove the free oscillation signals, SG records are bandpass filtered in the frequency range 0.1–0.2 mHz for comparison with the synthetic (Fig. 5). We do not present the STS-1Z records because of the lower sensitivity in this frequency band.

Calculated gravity variations for the tsunami generated by a simple fault model are comparable to the filtered SG record (Nawa *et al.*, 2007). Peak-to-peak amplitudes at approximately 1400 min after the earthquake are 1.5 μGal for the observation and 1.3 μGal for the synthetic from the tsunami source model (Fujii and Satake, 2007). Furthermore, the amplitudes in the period from 760 to 1960 min are 0.20 μGal for the observation and 0.25 μGal for the synthetic (Fig. 5a). The noise level of the SG in this frequency band is found to be less than 0.1 μGal.

Discussion

Comparison of the synthetic and observed data shows that amplitude discrepancies in both the STS-1 north–south and east–west components are larger than those in of BPG and SG records (Fig. 5a). Moreover, all the synthetic waves of the BPG, STS-1, and SG indicate that the phases are different compared to the observations. It is suggested that the discrepancies could be due to inaccuracies in the bathymetry data around the observation site employed in the computation.

To examine the effect of the accuracy of the bathymetry data, we attempted to simulate a tsunami using other bathymetry data. The sea level variations observed at Syowa Station are affected largely from bathymetry around the station. Even though the observed PSD of BPG2 is smaller than that of BPG1, the synthetic wave at BPG2 is more consistent with observation than at BPG1, as illustrated in Figure 4. Therefore, instead of using a global topography dataset (ETOPO2) in the vicinity of Syowa Station, we used water depth data digitized from the 1:250,000 bathymetric chart of Lützow–Holm Bay compiled by Moriwaki and Yoshida (1990). The new chart represents some drowned glacial troughs that are not revealed in ETOPO2 (Fig. 6). The grid size of the replaced bathymetry is the same as before: 10 min of the arc. The computation results for the new bathymetry are presented in Figure 5b.

Comparison of Figure 5a and b demonstrates that there is some improvement in the fit between the observed and synthetic waves because of the revised bathymetry data. The improvements are (1) for BPG1, the large amplitude variation after 1800 min in Figure 5a is significantly reduced and the consistency in the phase is also improved; (2) for both STS1 north–south and east–west, the amplitude difference between synthetics and observations is significantly reduced, especially in the east–west component; and (3) for SG, the synthetic waveforms are similar to observation, although there is still a discrepancy in the phase (Fig. 5b). The rms amplitudes of the synthetic waves in the frequency range 0.3–0.6 mHz in Figure 5b are 14.4 μGal and 6.2 μGal for the north–south and east–west components, respectively. These values are closer to the observed values of 7.9 μGal and 4.7 μGal, while those computed from ETOPO2 data are 20.1 μGal and 10.6 μGal.

As shown in the aforementioned comparison, the accuracy of the bathymetry data employed in the computation affects the results. The submarine topography of Lützow–Holm Bay seems to be more complicated than the ETOPO2 data. The synthetics need to be calculated using bathymetry data of a higher accuracy (Satake, 1995). However, submarine topography in the Antarctic continental margin is difficult to measure, which may be due to the existence of thick sea ice. Computation results indicate that the local effects within Lützow–Holm Bay are significant for both the attraction and loading effects at Syowa Station. Moreover, the tilt effects are sensitive to topography near the coast (Sato and Hanada, 1984). At frequencies higher than those employed in this study we would need to calculate synthetic waves for a higher resolution (smaller grid size) for a tsunami and the induced effects. This is a matter for future research.

In addition to the tilt effects, the horizontal components of STS-1 should also record displacements from the tsunami loading. Using the GOTIC program, we estimated acceleration amplitudes expected from horizontal displacements. As a result, the calculated acceleration amplitude from the tsunami loading, not the tilt effects, was found to be negligible (approximately 0.1 μGal: 10^{-9} m/sec^2). The amplitude of horizontal displacements is less than 1 mm for both the north–south and east–west components. The displacements may be too small in magnitude to detect from the continuous Global Positioning System (GPS) observation conducted at Syowa Station, a site of the International GPS Service (IGS) (Yamada *et al.*, 1998).

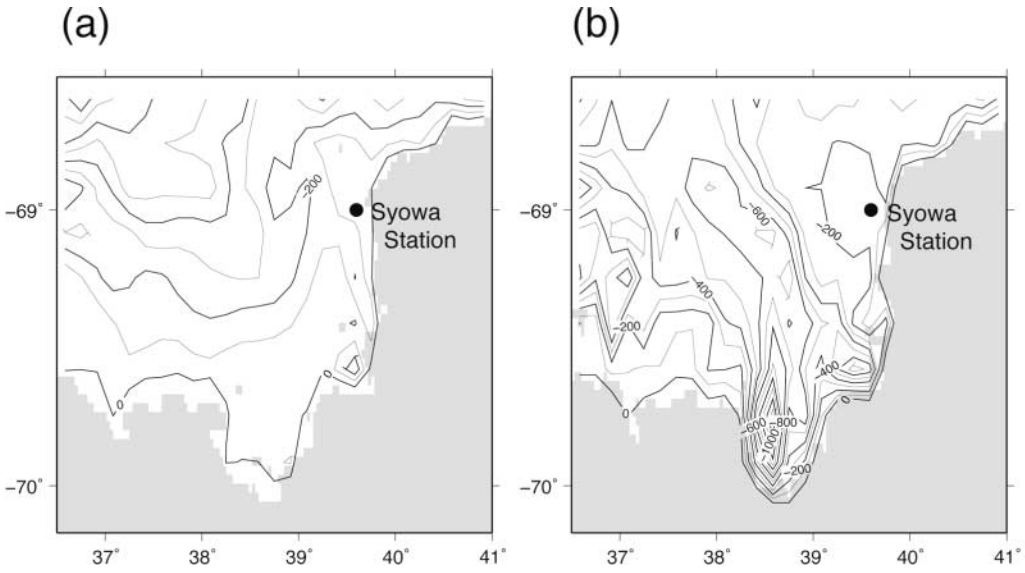

Figure 6. Contour map of bathymetry in the vicinity of Lützow–Holm Bay. (a) ETOPO2 and (b) ETOPO2 and detailed bathymetry from the 1:250,000 bathymetric chart compiled by Moriwaki and Yoshida (1990). Contour interval is 100 m.

Conclusion

The 2004 Indian Ocean tsunami was observed using STS-1H and SG at Syowa Station. The STS-1H and SG recorded the tilt and gravity effects of the tsunami, respectively. The rms amplitudes of tilt effects are 5 and 8 μGal in the east–west and north–south direction, respectively, from 20-hr-long STS-1 records in the frequency range 0.3–0.6 mHz. The rms amplitude of the gravity effect was found to be 0.2 μGal, obtained from SG records for the same time period in the frequency range of 0.1–0.2 mHz.

We compared the observed data with computational results of synthetic tsunami waves. As demonstrated in the comparison of the rms amplitudes between the observed and the synthetic tilt effects, the difference is improved when a detailed bathymetry model is used in the calculation. In order to estimate a source mechanism of the 2004 Sumatra–Andaman earthquake, to estimate a subsurface structure around the observation site, and to use the synthetic tsunami data as an input for the noise reduction of the Earth's free oscillation records, bathymetry data of greater precision would be required.

Acknowledgments

We would like to thank the Japan Coast Guard for obtaining and distributing the sea level data from Syowa Station, Antarctica. We are grateful to Professors. N. Ishikawa and Y. Nogi and the members of JARE45 and 46 for observations using ocean-bottom pressure gauges, broadband seismometers, and the superconducting gravimeter. We thank K. Sieh and reviewers for their comments, which improved our manuscript. A part of this work was conducted by Grants in Aid for Scientific Research of the Ministry of Education, Culture, Sports, Science, and Technology of Japan (Nos. 16310015, 16340134, 17540400).

References

Doi, K., K. Shibuya, Y. Nogi, and N. Ishikawa (2005). Observation by ocean bottom pressure gauges in the Antarctic Ocean, presented at Dynamic Planet 2005, Cairns, Australia, 22–26 August 2005, PTH0087.

Endo, T., and S. Okubo (1984). A correction to "partial derivative of Love numbers," *Bull. Geod.* **58,** 73–74.

Farrell, W. E. (1972). Deformation of the Earth by surface loads, *Rev. Geophys. Space Phys.* **10,** 761–797.

Fujii, Y., and K. Satake (2007). Tsunami source of the 2004 Sumatra–Andaman earthquake inferred from tide gauge and satellite data, *Bull. Seism. Soc. Am.* **97,** no. 1A, S192–S207.

Fukuda, Y., S. Iwano, H. Ikeda, Y. Hiraoka, and K. Doi (2005). Calibration of the superconducting gravimeter CT#043 with an absolute gravimeter FG5#210 at Syowa Station, Antarctica, *Polar Geosci.* **18,** 41–48.

Hanson, J. A., and J. R. Bowman (2005). Dispersive and reflected tsunami signals from the 2004 Indian Ocean tsunami observed on hydrophones and seismic stations, *Geophys. Res. Lett.* **32,** L17606, doi 10.1029/2005GL023783.

Ikeda, H., K. Doi, Y. Fukuda, Y. Tamura, and K. Shibuya (2005). Installation of the superconducting gravimeter CT(#043) at Syowa Station, Antarctica, *Polar Geosci.* **18,** 49–57.

Iyemori, T., M. Nose, D. Han, Y. Gao, M. Hashizume, N. Choosakul, H. Shinagawa, Y. Tanaka, M. Utsugi, A. Saito, H. McCreadie, Y. Odagi, and F. Yang (2005). Geomagnetic pulsations caused by the Sumatra earthquake on December 26, 2004, *Geophys. Res. Lett.* **32,** L20807, doi 10.1029/2005GL024083.

Kanao, M., K. Kaminuma, K. Shibuya, Y. Nogi, H. Negishi, Y. Tono, and T. Higashi (1999). New seismic monitoring observation system and data accessibility at Syowa Station (in Japanese with English abstract), *Nankyoku Shiryo* (*Antarctic Record*), **43,** no. 1, 16–44.

Le Pichon, A., P. Herry, P. Mialle, J. Vergoz, N. Brachet, M. Garces, D. Drob, and L. Ceranna (2005). Infrasound associated with 2004-2005 large Sumatra earthquakes and tsunami, *Geophys. Res. Lett.* **32,** L19802, doi 10.1029/2005GL023893.

Merrifield, M. A., Y. L. Firing, T. Aarup, W. Agricole, G. Brundrit, D. Chang-Seng, R. Farre, B. Kilonsky, W. Knight, L. Kong, C. Magori, P. Manurung, C. McCreery, W. Mitchell, S. Pillay, F. Schindele, F.

Shillington, L. Testut, E. M. S. Wijeratne, P. Caldwell, J. Jardin, S. Nakahara, F.-Y. Porter, and N. Turetsky (2005). Tide gauge observations of the Indian Ocean tsunami, December 26, 2004, *Geophys. Res. Lett.* **32,** L09603, doi 10.1029/2005GL022610.

Moriwaki, K., and Y. Yoshida (1990). Bathymetric chart of Lützow–Holmbukta (Lützow-Holm Bay), Special map series of the National Institute of Polar Research, No. 4, Scale 1:250,000.

Nawa, K., K. Satake, N. Suda, K. Doi, K. Shibuya, and T. Sato (2007). Sea level and gravity variations after the 2004 Sumatra Earthquake observed at Syowa Station, Antarctica, in *Dynamic Planet*, C. Rizos and P. Tregoning (Editors), International Association of Geodesy Symposia, Vol. 130, Springer, Berlin (in press).

Nawa, K., N. Suda, S. Aoki, K. Shibuya, T. Sato, and Y. Fukao (2003). Sea level variation in seismic normal mode band observed with on-ice GPS and on-land SG at Syowa Station, Antarctica, *Geophys. Res. Lett.* **30,** 1402, doi 10.1029/2003GL016919.

National Oceanic and Atmospheric Administration (NOAA) (2001). ETOPO2 Global 2-minute gridded elevation data, (CD-ROM), Vol. E1, National Geophysical Data Center.

Odamaki, M., Y. Michida, I. Noguchi, Y. Iwanaga, S. Ikeda, and K. Iwamoto (1991). Mean sea-level observed at Syowa Station, East Antarctica, *Proc. NIPR Symp. Ant. Geosci.* **5,** 20–28.

Odamaki, M., K. Suzuki, J. Ogata, T. Masuda, T. Imoto, S. Wakamatsu, E. Suzuki, K. Muneda, A. Nagano, and Y. Michida (2005). Off Sumatra Earthquake tsunami record observed at SYOWA station, Antarctica, in *The 25th Symposium on Polar Geosciences Program and Abstracts*, National Institute of Polar Research, Tokyo, Japan, 76–78 (abstract in Japanese)

Ozawa, I. (1961). On the observations of crustal strains due to Chile tide wave, *Disaster Prevention Res Inst Annu.* **4,** 36–44 (in Japanese with English abstract).

Pino, N. A., M. Ripepe, and G. B. Cimini (2004). The Stromboli Volcano landslides of December 2002: a seismological description, *Geophys. Res. Lett.* **31,** L02605, doi 10.1029/2003GL018385.

Satake, K. (1995). Liniear and nonlinear computations of the 1992 Nicaragua Earthquake Tsunami, *Pure Appl. Geophys.* **144,** 455–470.

Satake, K. (2002). Tsunamis, in *International Handbook of Earthquake and Engineering Seismology*, W. H. K. Lee, H. Kanamori, P. C. Jennings, and C. Kisslinger (Editors), Vol. 81A, Academic Press, Amsterdam, 437–451.

Sato, T., and H. Hanada (1984). A program for the computation of oceanic tidal loading effects 'GOTIC', *Publ. Int. Latitu. Mizusawa* **18,** 63–82.

Tanaka, Y., and T. Tanaka (1961). On the ground tilt and strain caused by the Chile tsunami, *Disaster Prevention Res. Inst. Annu.* **4,** 45–60 (in Japanese with English abstract).

Titov, V., A. B. Rabinovich, H. O. Mofjeld, R. E. Thomson, and F. I. Gonzalez (2005). The global reach of the 26 December 2004 Sumatra tsunami, *Science* **309,** 2045–2048.

Yamada, A., K. Maruyama, O. Ootaki, A. Itabashi, Y. Hatanaka, S. Miyazaki, H. Negishi, T. Higashi, Y. Nogi, M. Kanao, and K. Doi (1998). Analysis of GPS data at Syowa Station and IGS tracking stations, *Polar Geosci.* **11,** 1–8.

Yanagisawa, M., and T. Wakasugi (1984). Observations of crustal tilt and strain indeced by the load of the 1983 Nihonkai-Chubu Earthquake tsunami *J. Geod. Soc. Jpn.* **30,** no. 3, 204–212 (in Japanese with English abstract).

Yuan, X., R. Kind, and H. A. Pedersen (2005). Seismic monitoring of the Indian Ocean tsunami, *Geophys. Res. Lett.* **32,** L15308, doi 10.1029/2005GL023464.

Geological Survey of Japan, AIST
Tsukuba Central 7
1-1-1 Higashi, Tsukuba
Ibaraki 305-8567, Japan
nawa@ni.aist.go.jp
(K.N., K.S.)

Hiroshima University
Higashi-Hiroshima
Hiroshima 739-8526, Japan
(N.S.)

Building Research Institute
1 Tachihara, Tsukuba
Ibaraki 305-0802, Japan
(Y.F.)

National Astronomical Observatory
Hoshigaoka, Mizusawa
Iwate 023-0861, Japan
(T.S.)

National Institute of Polar Research
Kaga, Itabashi
Tokyo 173-8515, Japan
(K.D., M.K., K.S.)

Manuscript received 23 January 2006.